Vítor Carvalho,
***Paulo Cardoso,**
***Michael Belsley,**
****Rosa M. Vasconcelos,**
Filomena O. Soares

DEI, UM,
Azurém, Guimarães, Portugal,
E-mail: vcarvalho@dei.uminho.pt
fsoares@dei.uminho.pt

***DF, UM,**
Gualtar, Braga, Portugal,
E-mail: pjcardoso@fisica.uminho.pt
belsley@fisica.uminho.pt

****DET, UM,**
Azurém, Guimarães, Portugal,
E-mail: rosa@det.uminho.pt

Yarn Irregularity Parameterisation Using Optical Sensors

Abstract
This paper presents an original system to measure yarn diameter using coherent optical signal processing to eliminate the influence of hairiness over the output signal. The system consists of optical hardware to produce an image which characterises the yarn diameter and electronic hardware that converts the optical yarn diameter image into a proportional voltage. LabVIEW customised software was used to acquire and process the output voltage interfaced through a Data Acquisition Board. The system determines traditional commercial yarn irregularity parameters including Ud (Mean Deviation), CVd (Coefficient of Variation), SDd (Standard Deviation), types of irregularities, frequency diagrams and spectral analysis based on FFT (Fast Fourier Transform). Moreover, several other parameters were also obtained, such as DRd (Deviation Rate), IDRd (Integral Deviation Rate), spectral analysis based on FWHT (Fast Walsh Hadamard Transform) and FDFI (Fast Impulse Frequency Determination), and length of irregularities classified for an overall variation range. A parameterisation comparison between two yarns is presented.

Key words: *diameter measurement, yarn parameterisation, optical sensors, signal processing.*

Introduction

The yarn diameter measurement system (***Figure 1***) is based on a previously developed yarn hairiness measurement system using coherent optical signal processing [1 - 6].

The objective of the optical setup was to obtain a signal proportional to the yarn diameter in the final image plane (position of the photodiode is in ***Figure 1***). Coherent light from a HeNe (Helium – Neon) laser (visible red) is guided through an adjustable diaphragm (D) to ensure a good transverse spatial profile. After the diaphragm, the laser beam passes directly to the yarn through a two lens beam expander telescope (L1 and L2), placed in the object holder (O). The size of the final image is controlled by lenses L3 and L4.

To process the image, a custom fabricated spatial filter (F) was placed in the Fourier plane of L3, allowing only the low spatial frequencies in the image to propagate further (a low pass spatial Fourier filter), in contrast to the yarn hairiness measurement system, which uses a high pass spatial Fourier filter. This results in the yarn core, as well as, the laser light, which is not blocked by the yarn, eliminating the contours of the edges and associated hairs [7 - 10].

The objective of the electronic hardware is to obtain a voltage which can be related to the yarn diameter. The output of a trans-impedance amplifier [11] connected to the photodiode was read by a Data Acquisition Board (DAQ) from National Instruments [12]. However, as the intensity of the laser light, which is not blocked by the yarn, caused the saturation of the photodiode, we placed a linear polariser, which was adjusted to attenuate the laser light signal, before the photodiode. In order to obtain a better SNR (Signal to Noise Ratio), the polariser should be adjusted to a maximum signal, which does not cause photodiode saturation, when the yarn is placed. Moreover, the photodiode region which is not blocked by the yarn diameter can also be reduced to improve the SNR.

A yarn image resulting from the optical hardware, without the application of any spatial filter, is similar to ***Figure 2***.

Figure 2 shows that the laser light which is blocked by the yarn (yarn core, contours and hairiness) causes a black region in the laser beam projection. Therefore, if we consider the image without yarn, as reference (no blocked regions), and subtract the yarn image (with blocked regions), we obtain an image of only the yarn, which depends on its diameter. The

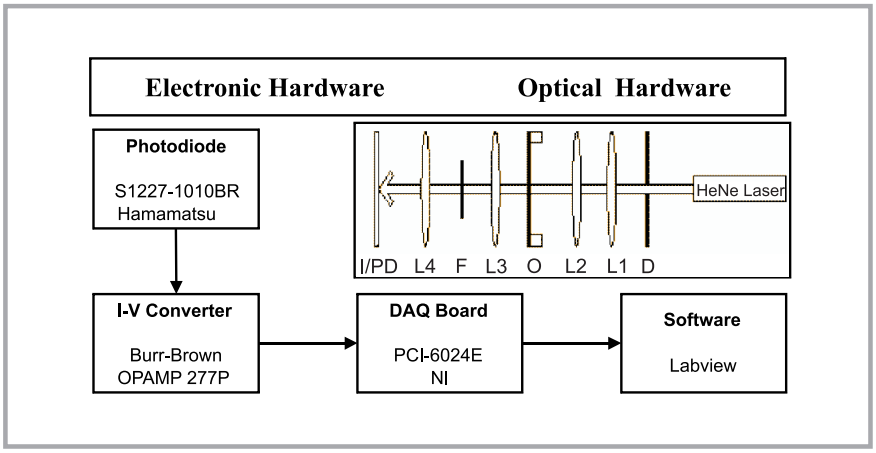

Figure 1. *Electronic and optical hardware used.*

Carvalho V., Cardoso P., Belsley M., Vasconcelos R. M., Soares F. O.; Yarn Irregularity Parameterisation Using Optical Sensors.
FIBRES & TEXTILES in Eastern Europe, January/March 2009, Vol. 17, No. 1 (72) pp. 26-32.

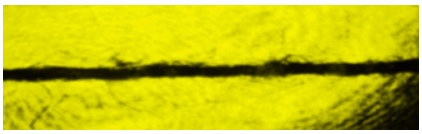

Figure 2. *Yarn image result without optical signal processing; clear visible is the hairiness.*

conversion of this light signal into a proportional voltage was performed using the previously developed electronic hardware (mainly a photodiode and trans-impedance amplifier). However, if we analyse ***Figure 2*** carefully, we can verify that yarn hairiness, which was already measured by the previously developed system [2 - 6], a significant amount of the laser beam signal can be blocked. To solve this problem, we used a low pass spatial optical filter in the Fourier Plane, with the same cut-off frequency as the high-pass filter applied in the hairiness measurement system, by which we should obtain the signal components (a yarn core and laser light that is not blocked by the yarn core), eliminating the unwanted influence of hairiness.

Figure 3 presents an example of images resulting from the application of a low pass spatial filter in which only the shadow of the yarn core is visible, while the small shadows due hairiness have been eliminated.

As diameter variations imply a linear change in yarn mass per unit length, this approach is appropriate to quantify the most common yarn irregularity parameters. Furthermore, as a high number of samples are taken over a single test, the average results for mass and diameter variations should be similar, considering that irregularities have a random distribution, and thus an equal probability of being orientated in any direction over the full 360° perpendicular to the yarn core. To confirm this claim, we carried out a study considering the signal obtained using a single direction. Then we carried out simultaneous measurements along two orthogonal directions by duplicating the optical and electronic hardware as well as correlating the results, which confirmed our theory [13].

Theoretical considerations

Irregularity statistical parameters

This section presents the statistical irregularity parameters measured by our system. Typical standard parameters available using commercial equipment include the number of irregularities, which are generally classified as [14 - 16] thick places – for mass increases (normally for values that are are least 40% above the average), thin places – for mass decreases (normally for values that are at least 40% below the average values) and neps - for huge mass increases (at least 100%). Our system quantifies the number of irregularities from zero to the maximum variation, in steps of 1%, adding also the length of irregularity, diameter variation, Ud (mean deviation), SDd (standard deviation), CVd (coefficient of variation) and frequency diagrams. In addition, our system introduces several new parameters, such as DRd (deviation rate) and IDRd (integral deviation-rate). All the parameters are measured considering the average diameter as a yarn reference [14].

Absolute mean deviation

The absolute mean deviation (U_d) corresponds to the deviation of the diameter from its average value. It is defined by equation (1).

$$U_d(\%) = \frac{100}{\overline{X}N}\sum_{i=1}^{N}\left|X_i - \overline{X}\right| \qquad (1)$$

where,

Table 1. *Linear mass of each yarn tested.*

Sample number	Linear mass, g/km
1	49.17
2	62.00
3	295.00

X_i – current sample diameter value,
$\overline{X}$ – average diameter value obtained during the evaluation time, and
N – number of samples.

Standard deviation

The standard deviation of the diameter is defined by equation (2).

$$SD_d(\%) = \sqrt{\frac{1}{N}\sum_{i=1}^{N}\left(X_i - \overline{X}\right)^2} \qquad (2)$$

Coefficient of variation

The coefficient of variation of the diameter (CV_d) is related to the standard deviation and the average value, as defined by equation (3).

$$CV_d(\%) = \frac{100}{\overline{X}}SDd \qquad (3)$$

Deviation rate

The deviation rate parameter, DR_d, measures the number of yarn samples with a diameter that is outside given limits relative to the average yarn diameter. To calculate the deviation rate, a function p(α, n) is defined which assumes the value of '1' if a sample is above or below these limits (α), and '0' if it is not, as quantified by equation (4).

$$p(\alpha,n) = \begin{cases} 1 & f & f(x) \geq \overline{X}(1+\alpha) \\ 0 & f & \overline{X}(1-\alpha) < f(x) < \overline{X}(1+\alpha) \\ 1 & f & f(x) \leq \overline{X}(1-\alpha) \end{cases} \qquad (4)$$

The deviation rate parameter, DR_d (%), is then a function of α as specified by equation (5).

$$DR_{d\alpha}(\%) = \frac{\sum_{i=0}^{N-1} p(\alpha,n)}{N}100 \qquad (5)$$

Integral deviation rate

The integral deviation rate parameter, IDR_d, calculates the absolute mean deviation for several thresholds (α). This parameter is measured using the function y(n), shown in equation (6).

$$y(n) = \begin{cases} \left|f(x) - \overline{X}(1+\alpha)\right| & f & f(x) \geq \overline{X}(1+\alpha) \\ 0 & f & \overline{X}(1-\alpha) < f(x) < \overline{X}(1+\alpha) \\ \left|f(x) - \overline{X}(1-\alpha)\right| & f & f(x) \leq \overline{X}(1-\alpha) \end{cases} \qquad (6)$$

It is defined as a function of α in equation (7):

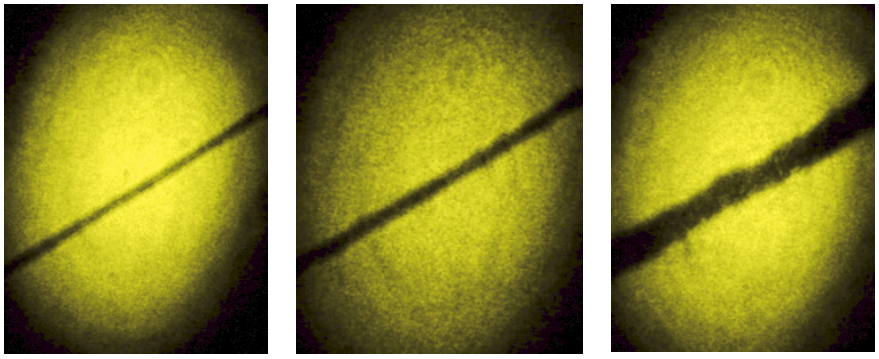

Figure 3. *Examples of images resulting from the application of a low-pass spatial filter; on order to eliminate the images of hairiness.*

$$IDR_{d\alpha}(\%) = \frac{\sum_{i=0}^{N-1} y(n)}{\overline{XN}} 100 \quad (7)$$

According to the definition, if α is zero, IDR_d equals the value of U_d. Thus, with IDR_d it is possible to quantify this characteristic (U_d) not only for 0%, but also for values in the range of [0, max. variation] in %, giving more complete information regarding diameter variations of the yarn in all limits.

Frequency of the diameter

Frequency diagrams calculate the histogram of diameter variation for certain predefined variation intervals in the range [min. variation, max. variation] in %.

Approaches to signal processing

In the spectral analysis of yarn diameter, three different approaches were used. The first is the traditional FFT (Fast Fourier Transform) for considering only real values, to test for the occurrence of sinusoidal patterns. The second is the FWHT (Fast Walsh Hadamard Transform) [5], which is computationally faster than the FFT, for detecting rectangular patterns. Lastly, the FDFI (Fast Impulse Frequency Determination) [14, 17], which can be used to detect impulse patterns. The FFT and FWHT use energy bands which integrate the harmonics within a certain interval, reducing the overlapping influence on the results. Moreover, this integration yields a result more readily understood by the yarn producer. Wavelengths are calculated considering results of frequency as in equation (8) [14, 15].

$$\lambda(m) = l\frac{f_a}{1000 f_d} \quad (8)$$

where,

l - width of sensor, mm,

f_a - acquisition frequency, Hz, and

f_d - detected frequencies, Hz.

Table 2. *Relationship between yarn diameters and average signals.*

Yarn linear mass, g/km	Average signal, V	Maximum diameter, mm	Minimum diameter, mm
49.17	0.2320	0.384	0.314
62.00	0.3265	0.518	0.460
295.00	0.6687	1.210	0.940

Table 3. *Percentage relationship between average signals and diameters.*

Proportionalities tested	Average signal variation, %	Maximum diameter variation, %	Minimum diameter variation, %
49.17/62.00	71.06	74.13	68.26
62.00/295.00	48.83	42.81	48.94

Experimental results

Yarn diameter characterisation

Three 100% cotton yarns with different linear masses were analysed. ***Table 1*** presents the linear masses of each yarn measured .

To ensure a 1mm analysis, a window aperture with an area of 1 mm × 4 mm was built in the photodiode. However, as the optical hardware produced a reduction of 54% in the image plane, a 1mm high window in the image plan corresponds to an effective height of 1 mm/0.54 = 1.85 mm in the object plane. A 4 mm wide window was used to allow for a possible oscillation of the sample yarn However, the yarn position was very stable, and it can be stated that a high percentage of samples were acquired in the centre of the laser beam where the window was placed, allowing reliable measurements (laser zone with high linearity).

We acquired 6k samples in steps of 1mm for each yarn. The value for calibration corresponding to the signal without yarn was 2.63 V. Afterwards, the difference between the acquisition signal and reference value was calculated in order to obtain an effective signal blocked by the yarn. ***Figure 4*** presents the results obtained.

Figure 4 shows, as expected, that higher linear mass yarns and, consequently, larger diameter yarns produce a greater number of blocked signals. ***Table 2*** presents the maximum and minimum diameters of each analysed yarn determined using images from an electron microscope, as well as the average value of their blocked signals.

As stated before and now confirmed by ***Table 2***, yarn linear masses are correlated with the yarn diameter. Furthermore, ***Table 2***, also shows that the average signal obtained has a direct proportionality with the yarn diameters.

Figure 5 presents the average diameter as a function of the average signal voltage for each yarn.

There is a clear tendency for a linear relationship between the yarn diameter and the average signal blocked by the yarns under test, with the least squares linear fit having an R squared value very close to one (0.9994). ***Table 3*** presents the percentage variation between the different yarns tested, considering their average signals and diameters. Calculi were performed

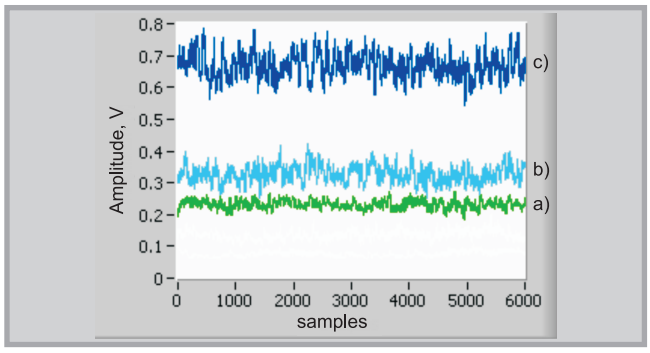

Figure 4. *Yarn blocked signals for each yarn analysed.*

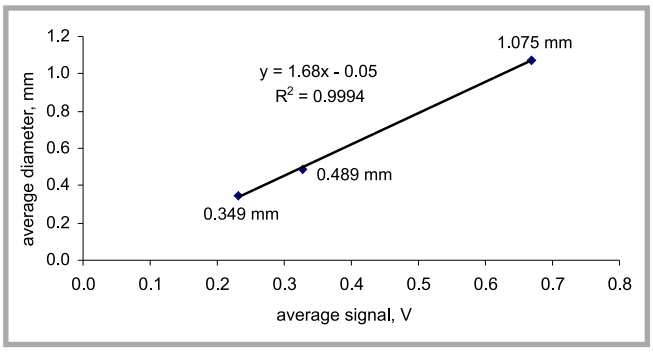

Figure 5. *Linear relationship between the average diameter and average voltage signal.*

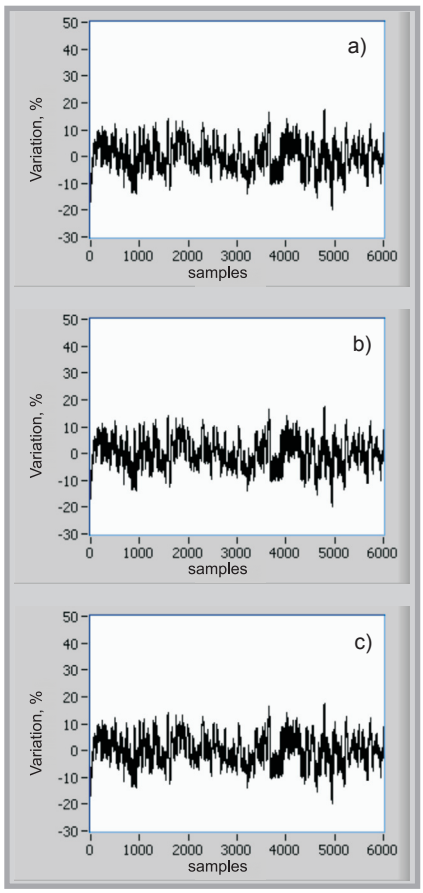

Figures 6. *Percentage variation signals of yarns a) 49.17 g/km, b) 62.00 g/km and c) 295.00 g/km, respectively, over the average.*

between each single parameter, namely, the minimum(49.17)/minimum(62.00) and minimum(62.00)/minimum(295.00), maximum(49.17)/maximum(62.00) and maximum(62.00)/maximum(295.00), and the average signal(49.17)/average signal(62.00) and average signal(62.00)/average signal(295.00).

Table 3 shows that the average variation signal in % is always in the same range of the diameter variation intervals, which further shows that there is a signal variation proportional to the yarn diameter.

Subsequently, we determined the blocked signal for each yarn as well as the percentage of variation referenced to the average blocked signal. ***Figure 6*** presents the values obtained for 49.17, 62.00 and 295.00 g/km yarns, respectively.

Examining ***Figure 6***, the yarn which seems to be more irregular is the 62.00 g/km, followed by the 295.00 g/km, due to their higher amplitude variations. The most regular seems to be the 49.17 g/km due to the inferior amplitude variation in comparison to the others. However, to confirm these observations, we determined the SD for each signal, as presented in ***Table 4***.

Table 4 confirms the previous observations that the 62.00 g/km yarn has the highest SD, being the most irregular yarn, followed by the 295.00 g/km yarn with an SD of 5.89%. The most regular is the 49.17 g/km yarn, with the lowest SD value (5.41%).

Parameter comparison between the 49.17 and 62.00 g/km yarns

Statistical Results

Yarn parameter characterisation was evaluated for the yarn blocked signals considering the values of U_d, CV_d, DR_d and IDR_d, the diameter frequency diagrams, as well as the number and length of irregularities in all the sensitivity range and signal processing analysis based on FFT, FWHT and FDFI, .

Table 5 shows the values of U_d and CV_d determined considering the blocked signals of yarns 49.17 g/km and 62 g/km.

As expected, the 49.17 g/km yarn presents amplitude values of U_d and CV_d inferior to the 62.00 g/km yarn, which are a result of its lower dispersion range (***Figure 6***). Moreover, a relationship of approximately 1.25 is obtained between U_d and CV_d for both yarns. This was also verified in the traditional yarn mass measurements using capacitive sensors [14 - 16]. Furthermore, the values of CV_d are similar to those obtained in table 4 for *SD*. This happens because, according to the definition, calculating the *SD* of the percentage variation signal over the average is the same as calculating the *CV* of the yarn blocked signal.

Table 4. *SD results obtained for percentage variation signals of each yarn.*

Yarn sample, g/km	SD of variation signal, %
49.17	5.41
62.00	7.87
295.00	5.89

Table 5. *Results of U_d, CV_d and their relationship.*

Quantity	49.17 g/km	62.00 g/km
Ud, %	4.40	6.36
CVd, %	5.41	7.87
CV/Ud	1.23	1.24

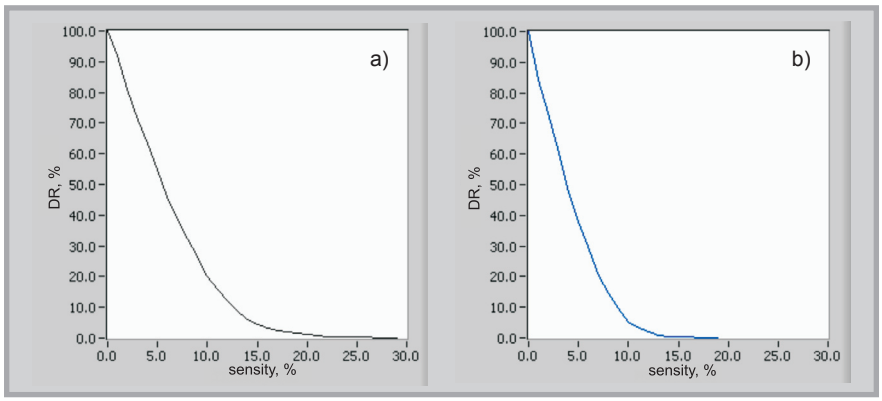

Figure 7. *DR results for the yarns considered; a) 62.00 g/km, b) 49.17 g/km.*

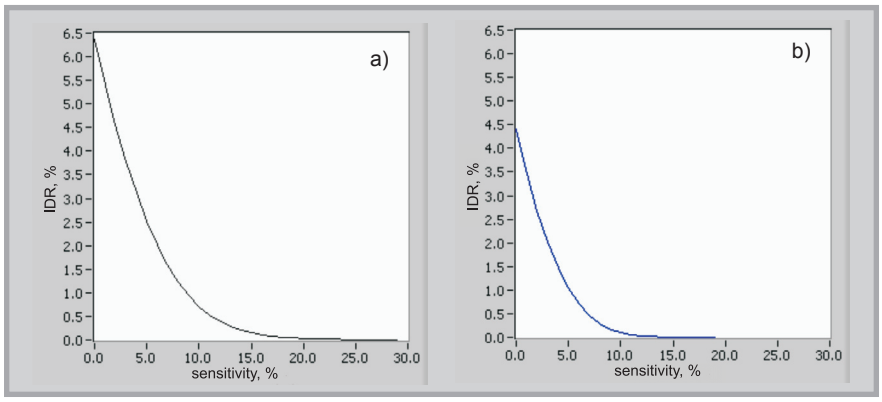

Figure 8. *IDR results for the yarns considered; a) 62.00 g/km, b) 49.17 g/km.*

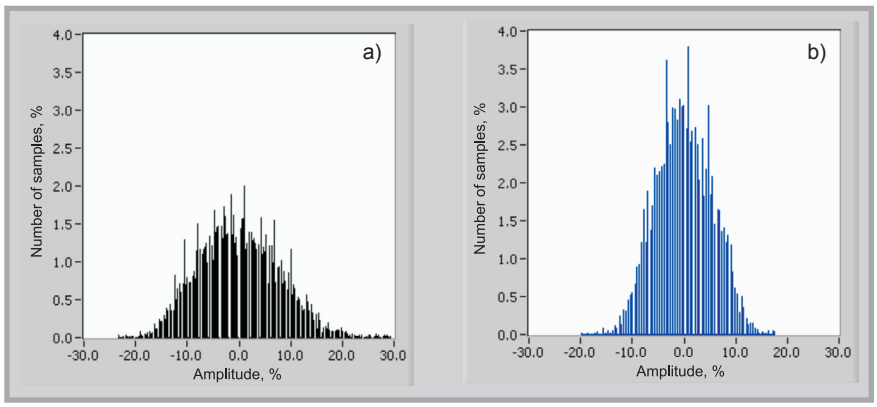

Figure 9. *Results of frequency diameter variation for the yarns considered; a) 62.00 g/km, b) 49.17 g/km.*

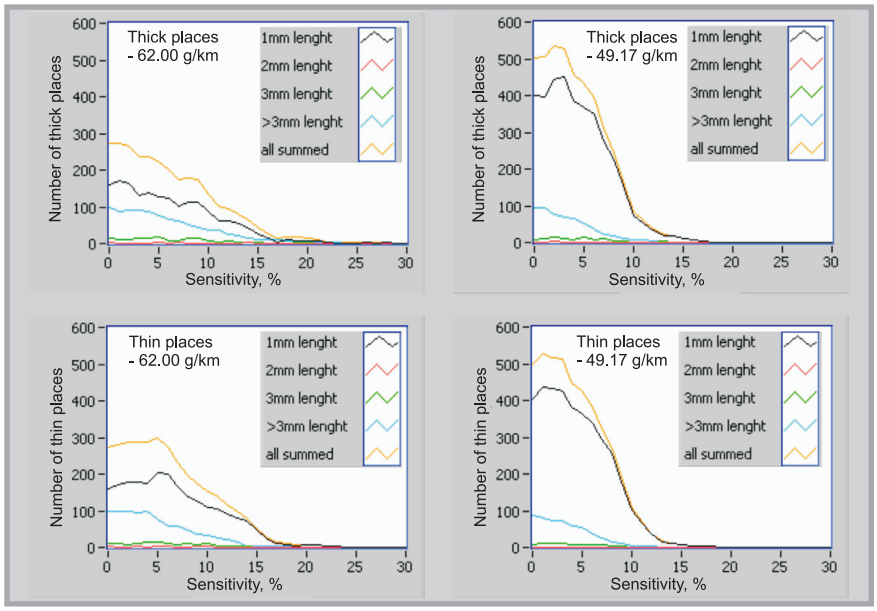

Figure 10. *Irregularity results for the yarns considered*

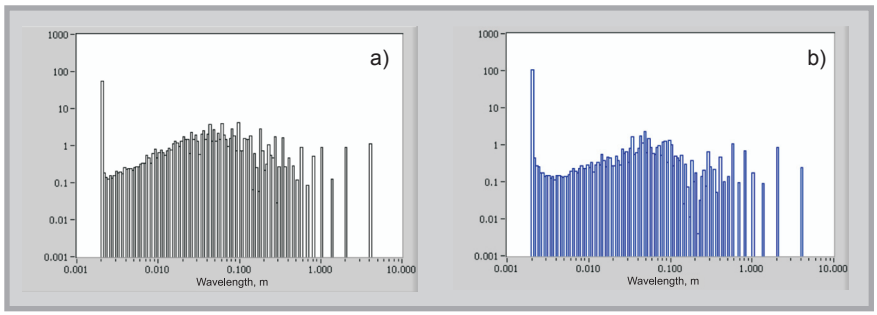

Figure 11. *FFT spectograms obtained for the yarns compared; a) 62.00 g/km, b) 49.17 g/km.*

Afterwards, we determined the DR_d and IDR_d for both yarn samples. ***Figures 7*** and ***8*** presents the results of DR_d and IDR_d obtained, respectively.

Observing the *DR* values of both yarns, one sees that the more regular yarn (49.17 g/km) decays more quickly with increasing sensitivity. In the *DR* analysis, the more regular the yarn is, the faster it will decay with increasing sensitivity, or equivalently the smaller the area under the DR curve, the lower the area is.

Observing the *IDR* curves of both yarns, we can confirm that the *IDR* values for a sensitivity of 0%,equal the values of U_d, as they should according to the definition. Secondly, the amplitude of the more regular yarn (49.17 g/km) is always lower for a given sensitivity range. A faster variation of the curve was also obtained, as stated in the DR analysis.

Figure 9 presents diameter variation frequency diagrams obtained for yarns 62 g/km and 49.17 g/km, respectively.

Comparing both frequency diagrams, it is verified that the 62 g/km yarn has a wider curve than the 49.17 g/km yarn, with a lower central (near 0%) amplitude. The reason for this is that as the 49.17 g/km yarn is more regular, a higher concentration of samples is positioned near the 0% values, resulting in a narrower curve with a higher central amplitude. A perfect yarn should have the totality of samples (100%) positioned in the 0% amplitude.

Figure 10 presents irregularity results for the yarns compared. Only thick and thin places are shown because no neps were identified in either of the sample yarns.

Considering ***Figure 10***, some similarities are evident in all the graphics: thick places occur in larger numbers than thin places; the number of irregularities is ordered in terms of occurrence by 1 mm, >3 mm, 3 mm and 2 mm length analysis. As expected, for 0% sensitivity, the number of thin points equals the number of thick points for each yarn in all lengths.

Comparing the irregularity results of both yarns, it is observed that a faster variation in curves, as stated before in DR_d and IDR_d analyses, is also observed for the more regular yarn (49.17 g/km); a larger number of irregularities was detected up to 8% sensitivity in the regular yarn (49.17 g/km), beyond 9% the tendency is reversed; for lower sensitivities the number of irregularities is not directly correlated with the regularity of the yarn.

Finally, as this characterisation was performed using only a single projection onto one photodiode, a factor of 1.57 in the irregularity values, it should be considered a valid approximation, as confirmed earlier [13], for the total number of irregularities in a full (360 degree) characterisation.

Signal processing results

Figure 11 presents signal processing results based on FFT for the sample yarns tested.

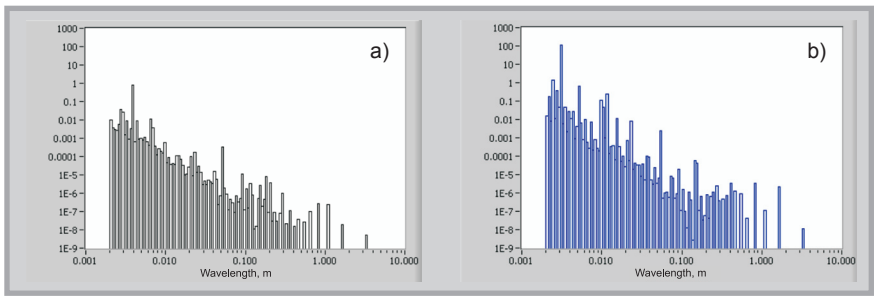

Figure 12. *FWHT spectograms obtained for the yarns compared; a) 62.00 g/km, b) 49.17 g/km.*

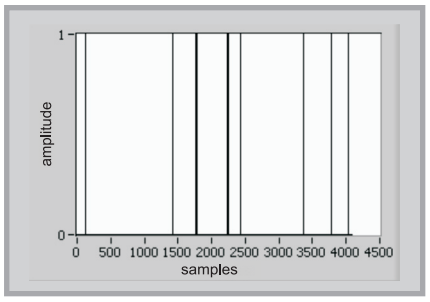

Figure 13. *FDFI error signal generated.*

Observing both FFT spectrums, one can note a high amplitude sinusoidal band in the 2 mm wavelength, which is caused by the slight oscillation of the yarn being tracked over the test. No more high protruding peaks were detected over the spectrum; however, for the 62.00 g/km yarn a higher number of medium amplitude protruding peaks is observed between 4 cm and 1 m. This is verified because, being a more irregular yarn, its higher signal dispersion is reflected over the spectrum, as the amplitude variations are superior and more pronounced in comparison to the more regular yarn.

Figure 12 presents the signal processing results based on FWHT.

Examining both FWHT spectrums, we conclude that:

- The regular yarn (49.17 g/km) has, in general, a higher amplitude, because a good match of rectangular periodical patterns were determined, as verified by the superior number of local peaks; highly regular yarns more easily match the patterns tested by FWHT, and as a consequence their spectra have more protruding bands and a higher general amplitude in comparison to the FFT spectra. This explains why we generally detect, for the same wavelengths, protruding bands with different amplitudes. As FFT is a sinusoidal based technique, rectangular signals are recognised in several wavelengths and, thus, are spread out with lower amplitudes than in FWHT. The opposite could also occur, as observed in the sinusoidal yarn oscillation band detected in the FFT on a single band, which is divided into several bands with lower amplitudes in the FWHT, between 2 mm and 1 cm.
- In the log-log scale, there is a linear relationship between the amplitude and wavelengths.

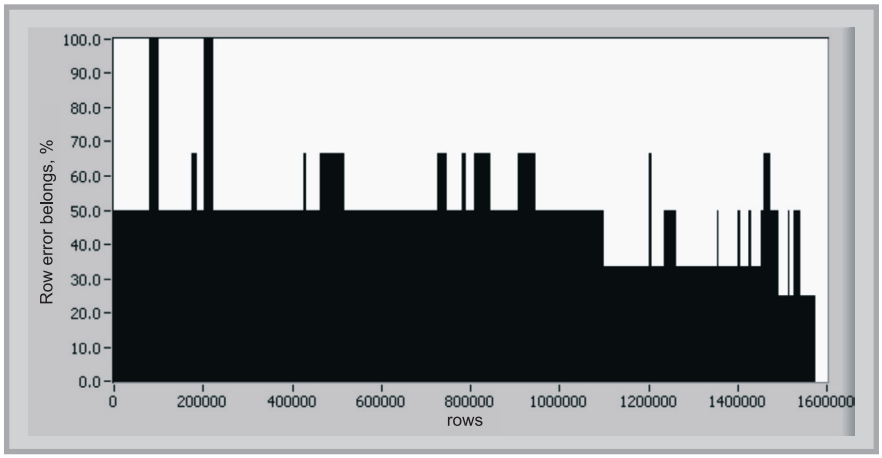

Figure 14. *Belonging results of the FDFI row errors.*

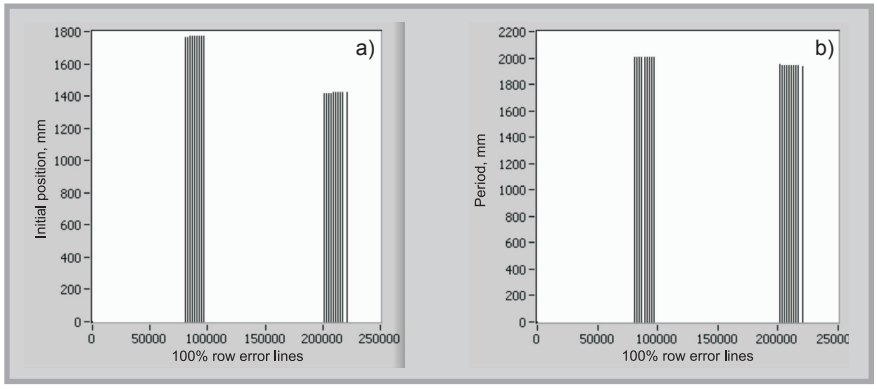

Figure 15. *Initial position of the 100 % row error lines and period; a) 62.00 g/km, b) 49.17 g/km.*

Figures 13 to ***15*** presents the signal processing results based on FDFI tested for impulse errors superior to 20% or inferior to -20%.

As the 49.17 g/km yarn does not have variations superior to the defined ranges, no impulse errors were obtained for these thresholds. ***Figures 13*** to ***15*** represent the results obtained for the 62.00 g/km yarn, where impulse errors were obtained.

Figure 13 presents the error signal generated.

In ***Figure 13*** the error signal is distributed over the full range of test samples in accordance with the threshold defined, because the source signal (Figure 6) has variations of 20% or greater over the error signal samples identified.

The error signal was subsequently tested with 1573376 periodical impulse errors resulting from $((N/2+N/4+1)/2\times(N/2-N/4))$ [6, 7], where N is the number of samples tested (4096).

The signal of row error matches is presented in ***Figure 14***.

Table 6. *Description of 100% error lines.*

100% row error index	initial position, mm	period, mm	number of impulses
80897	1766	2009	2
82907	1767	2008	2
84916	1768	2007	2
86924	1769	2006	2
88931	1770	2005	2
90937	1771	2004	2
92942	1772	2003	2
94946	1773	2002	2
96949	1774	2001	2
201265	1415	1948	2
203213	1415	1947	2
205160	1415	1946	2
205162	1417	1946	2
207108	1417	1945	2
209051	1415	1944	2
209053	1417	1944	2
209055	1419	1944	2
210999	1419	1943	2
212940	1417	1942	2
212942	1419	1942	2
212944	1421	1942	2
214886	1421	1941	2
216825	1419	1940	2
216827	1421	1940	2
220706	1421	1938	2

Observing ***Figure 14***, one can identify periodic impulse errors because 100% of the error occurrences are represented, which are clearly identified in ***Table 6***.

Considering the periodic impulse errors determined, ***Figure 15*** represents their initial position and period, respectively, which are also clearly identified in ***Table 6***.

Table 6 presents the identification of indexes of 100% row errors, their respective initial positions, period and number of impulses.

Considering ***Table 6***, we can verify that the 100% row error lines are placed between error line indexes 80897 and 220706, with initial positions between 1421 mm and 1774 mm and periods between 1938 mm and 2009 mm. It is also seen that all the impulse errors detected have 2 impulses.

Conclusions and future work

Considering the above study we can conclude that the presented methodology (coherent optical signal processing plus additional electronics and software) obtains reliable results in the determination of yarn diameter variation.

Hence, considering the statistical parameterisation (U_d, SD_d, CV_d, DR_d, IDR_d, frequency diagrams and irregularities), it is possible to determine the level of regularity of the yarn over the sample analysed .

The determinations of irregularities for several thresholds are of utmost importance as they can be used to improve the quality level of the yarn when considering values under the traditional thresholds.

The use of several signal processing approaches leads to more accurate and precise error identification - FFT clearly identifies sinusoidal error patterns, FWHT clearly identifies rectangular wave patterns and FDFI impulse error patters, which are not detected by the techniques already known. Thus, if the signal analysed has variations that are better approximated by sinusoidal waves, it is expected to obtain larger amplitudes using the FFT approach (or vice-versa). As the FDFI result is obtained in a row error below the graph, it is easy to verify if a periodical impulse error, which is tested over all possibilities by a specific matrix [14, 17], has occurred (row error belonging at 100%).

This work is part of a R&D project to develop an automatic system to characterise yarn quality, to measure irregularities, hairiness and production yarn characteristics, which integrates both optical and capacitive sensors [14, 18], as well as image processing techniques. With the extensive number of parameters that are potentially available, it is expected that the system developed, which is both reliable and affordable, will significantly increase the information accessible to yarn textile manufacturers.

Acknowledgment

The authors are grateful to the Portuguese Foundation (FCT) for funding through a scholarship (BD/19028/2004).

References

1. *Carvalho V., Cardoso P., Belsley M., Vasconcelos R., Soares F.; "Yarn Diameter Measurement Using Coherent Optical Signal Processing" IEEE Sensors Journal, Vol. 8, Issue 11,November 2008, pp1785-1793.*
2. *Carvalho V., Cardoso P., Belsley M., Vasconcelos R., Soares F.; "Determination of Yarn Hairiness Using Optical Sensors", EUROSENSORS XX, 17-19 September, Gothenburg, Sweden, 2006.*
3. *Carvalho V., Cardoso P., Belsley M., Vasconcelos R., Soares F.; "Development of a Yarn Evenness Measurement and Hairiness Analysis System", IECON06, 7-10 November, Paris, France, 2006.*
4. *Carvalho V., Cardoso P., Belsley M., Vasconcelos R., Soares F.; "Yarn Hairiness Parameterization Using a Coherent Signal Processing Technique", Sensors and Actuators A, Vol. 42, Issue 1, March 2008, pp. 217-224.*
5. *Carvalho V., Cardoso P., Belsley M., Vasconcelos R., Soares F.; "A New Statistical Reference Method for Yarn Hairiness Quantification", ISIE 2007, 4-7 June, Vigo, Spain, 2007.*
6. *Carvalho V., Cardoso P., Belsley M., Vasconcelos R., Soares F.; "Optical Yarn Hairiness Measurement System", INDIN07, 23-27 July, Vienna, Austria, 2007.*
7. *Goodman J.W., Introduction to Fourier Optics, McGraw-Hill, Greenwood Village, 1996.*
8. *Steward E.G., Fourier Optics: An Introduction, Dover Publications, New York, 2004.*
9. *Duffieux P.M., The Fourier Transform and its Applications to Optics 2nd Edition, John Wiley & Sons, New York, 1983.*
10. *Madsen C.K., Optical Filter Design and Analysis: A Signal Processing Approach, Wiley-Interscience, New York, 1999.*
11. *Franco S., Design with Operational Amplifiers and Analog Integrated Circuits, 3rd Edition, Mc-Graw Hill, Greenwood Village, 2001.*
12. *www.ni.com*
13. *Carvalho V., Belsley M., Vasconcelos R., Soares F.; "Yarn Diameter Characterization Using Two Orthogonal Directions", (accepted for publication in Journal Experimental Techniques).*
14. *Carvalho V., Parametrização de Fio Têxtil Baseada na Análise de Massa., Msc Thesis, Minho University, Guimarães, Portugal 2002.*
15. *Furter R., Evenness Testing in Yarn Production: part I, The Textile Institute and Zellweger Uster AG, Manchester: 1982.*
16. *Neves J. S.; A Irregularidade dos Fios Têxteis, sua origem, medição e análise, Oporto: 1968.*
17. *Monteiro J. L., Couto C.; "Pulse frequency calculation and estimation in yarn evenness analysis", IEEE Industrial Electronics Society, Orland, USA, 1995.*
18. *Baxter L.; Capacitive Sensors: Design and Applications, IEEE Press, NJ: 1997.*

Received 31.07.2007 Reviewed 02.07.2008